CCFE
CULHAM CENTRE FOR FUSION ENERGY

UK Atomic Energy Authority

UKAEA-CCFE-PR(21)81

D. Brunetti, C. J. Ham, S. Saarelma, J. P. Graves, J. W. Connor, A. Kleiner

Finite magnetic well effects on resistive and drift-resistive ballooning modes in a shaped tokamak

Finite magnetic well effects on resistive and drift-resistive ballooning modes in a shaped tokamak

D. Brunetti, C. J. Ham, S. Saarelma, J. P. Graves, J. W. Connor, A. Kleiner

This is a preprint of a paper submitted for publication in Nuclear Fusion

Finite magnetic well effects on resistive and drift-resistive ballooning modes in a shaped tokamak

D. Brunetti,[1,*] C. J. Ham,[1] S. Saarelma,[1] J. P. Graves,[2] J. W. Connor,[1] and A. Kleiner[3]

[1]UKAEA-CCFE, Culham Science Centre, Abingdon, Oxon, OX14 3DB, United Kingdom
[2]École Polytechnique Fédérale de Lausanne (EPFL),
Swiss Plasma Center (SPC), CH-1015 Lausanne, Switzerland
[3]Princeton Plasma Physics Laboratory, Princeton University, Princeton, New Jersey 08543, USA

(Dated: October 14, 2021)

The impact of plasma shaping through magnetic well modifications on the stability of resistive ballooning modes in tokamaks is analysed, also including finite diamagnetic flows. Various limiting cases of the dispersion relation, obtained by matching the averaged ballooning equation across the ideal and resistive layers, are analysed. It is found that stability is generally improved by the combination of vertical elongation and positive triangularity, although, in some cases, the growth rate of the unstable mode can be enhanced by these effects. Usually, vertically elongated plasmas with no triangularity are prone to exhibit worse stability properties. A value for the critical β above which resistive ballooning modes are driven unstable is identified, and a connection with type-III ELM activity is established.

I. INTRODUCTION

H-mode tokamak plasmas are typically characterised by an edge transport barrier [1, 2], in which temperature and density abruptly decrease within a narrow region. As such, large pressure gradients develop which in turn destabilise edge fluctuations called Edge Localised Modes (ELMs). One of the mechanisms that limit the achievable pedestal height is the cycle of pressure drop and subsequent recovery due to ELMs destabilisation. Various types of ELMs are observed depending on pedestal parameters (i.e. temperature and density) [3], the most dangerous ones being the so called type-I ELMs. These events are associated with violent eruptions of energy and particles which deposit significant heat loads on the plasma facing components (PFCs). These heat loads will be intolerable for a steady state reactor and significant research efforts have been directed at developing scenarios without type-I ELMs.

In the eventuality that ELMs cannot be avoided, an ELMy scenario which could potentially be compatible with reactor conditions is the type-III ELMy operating regime [4–6]. Type-III ELMs are characterised by a high repetition rate associated with modest heat and particle loads on the PFCs, and are usually observed above the $L \rightarrow H$ transition boundary [7, 8] at high pedestal collisionality [3, 9–11]. A coherent magnetic precursor oscillation of toroidal mode number $n \approx 5 - 15$ is often observed [11–14]. These perturbations tend to occur below the marginal boundary of peeling ballooning modes and disappear as the input power, and therefore temperature, is increased [9, 12]. This suggests that type-III ELMs may be resistive in nature, and indeed several works pointed to the importance of resistive effects on edge modes [15–18].

The most likely magnetohydrodynamic (MHD) instabilities that could explain such behaviour are the resistive ballooning modes (RBMs) [7, 19]. Contrarily to ideal ballooning modes which exhibit two stability regions one at low and the other at high pressure (*first* and *second* stability regions respectively) [20, 21], RBMs are generally found to be unstable all the way across the first ideal stability region [22, 23], whereas they are mainly stable in the second one. This would predict that they should be always observed if the pressure is sufficiently low, which is in contrast with experimental observations [7]. However, an island of stability at low pressure can be accessed if finite magnetic well corrections are included [20, 24–27]. These contributions, which are stronger for moderate n values typically associated with type-III ELM precursors [11–14], may therefore have a significant role. It is important to point out that plasma shaping has a strong impact on the magnetic well [28, 29] improving the pedestal performances, and indeed higher pedestal pressures were sustained at high triangularity in type-I and type-III ELMy regimes [7, 30]. Additionally, diamagnetic flows are known as an important stabilisation mechanism, and these are likely to be generated in the pedestal where strong gradients develop in H-mode scenarios.

Hence, the aim of this paper is to investigate the role of magnetic well effects, primarily through plasma shaping, on the stability of RBMs, providing a physical understanding of the type-III ELM phenomenon and potentially a scaling for the pedestal height. Indeed, the accessibility of a stability window in the ideal ballooning first stable domain, i.e. at low pressure, could explain why type-III ELMs are observed after the pedestal pressure reaches a threshold value and not before. Note also that the type-III ELMs high repetition rate is likely to be associated with a lower pressure threshold driving the instability [11]. The analytical calculations presented in this work also include finite Larmor radius (FLR) corrections, which may become significant when strong edge gradi-

* Electronic address: daniele.brunetti@ukaea.com

ents (in temperature and density) develop and for sufficiently large n toroidal mode numbers (even for moderate diamagnetic flows). Finally, by employing the EPED model [31, 32] for the pedestal width, we aim to derive an explicit expression, which depends upon macroscopic plasma parameters e.g. pedestal temperature and density, of the RBM marginal boundary. Hence, we identify the type-III ELMs boundary in the density-temperature parameter space, by linking them to RBM, and to some extent ideal ballooning mode, dynamics.

Thus, the paper is organised as follows: In section II the MHD model and plasma equilibrium for a shaped tokamak are discussed. The derivation of the averaged ballooning equation is discussed in section III, in which a two-region analysis is carried out. The discussion of various limiting cases for the stability boundaries obtained from the dispersion relation, which closely follows the approach of Refs. [33, 34], is the main aim of section IV, and the connection of the analytical results with the experimental observation of type-III ELMs activity is proposed in section V. Finally, in section VI a discussion of the results and future outlook is given.

II. MHD MODEL AND EQUILIBRIUM

It is convenient here to provide a brief summary of the physical framework within which the stability analysis will be carried out. Plasma evolution is assumed obeying the resistive drift-MHD equations [35, 36]:

$$\rho\left(\partial_t \boldsymbol{v} + \boldsymbol{v}\cdot\boldsymbol{\nabla}\boldsymbol{v} + \boldsymbol{v}^*\cdot\boldsymbol{\nabla}\boldsymbol{v}_\perp\right) = -\boldsymbol{\nabla}p + \boldsymbol{J}\times\boldsymbol{B}, \tag{1}$$

$$\partial_t \boldsymbol{B} = \boldsymbol{\nabla}\times(\boldsymbol{v}\times\boldsymbol{B}) - \eta\boldsymbol{\nabla}\times\boldsymbol{J} + \frac{m_i}{e_i}\boldsymbol{\nabla}\times\left(\frac{\boldsymbol{\nabla}_{||}p_e}{\rho}\right), \tag{2}$$

$$\partial_t p + \boldsymbol{v}\cdot\boldsymbol{\nabla}p + \tfrac{5}{3}p\boldsymbol{\nabla}\cdot\boldsymbol{v} = 0, \tag{3}$$

$$\partial_t \rho + \boldsymbol{\nabla}\cdot(\rho\boldsymbol{v}_i) = 0, \tag{4}$$

where $\boldsymbol{v}$ and $\boldsymbol{v}^* = m_i\boldsymbol{B}\times\boldsymbol{\nabla}p/(e_i\rho B^2)$ (m_i and e_i are the ion mass and electric charge) are the plasma MHD and ion diamagnetic velocities respectively with $\boldsymbol{v}_i = \boldsymbol{v} + \boldsymbol{v}^*$, ρ is mass density, $\boldsymbol{J} = \boldsymbol{\nabla}\times\boldsymbol{B}$ the current density having normalised $\mu_0 = 1$, p_i and p_e the ion and electron pressure respectively with the total pressure denoted by p and η the plasma resistivity which is assumed constant. The symbol $\perp$ indicates the vector perpendicular projection to the magnetic field, i.e. $\boldsymbol{v}_\perp = \boldsymbol{B}\times(\boldsymbol{v}\times\boldsymbol{B})/B^2$. Here we assume that the plasma is sufficiently collisional so that at equilibrium $T_e = T_i$. Note that the high collisionality assumption allows us to neglect bootstrap corrections to the total toroidal current. We point out that in equation (2) we assumed $\boldsymbol{B}\cdot\boldsymbol{\nabla}T_e \approx 0$.

Let us consider a large aspect ratio tokamak ($\varepsilon = a/R_0 \ll 1$ where R_0 and a are the major and minor radii respectively) with a D-shaped cross-section [37]. Let (r,ϑ,φ) be a right handed coordinate system with r a flux label with the dimensions of length, and ϑ (counter-clockwise) and φ the poloidal and toroidal angles respectively. The equilibrium magnetic field in the plasma is $\boldsymbol{B} = F\boldsymbol{\nabla}\varphi - \boldsymbol{\nabla}\psi\times\boldsymbol{\nabla}\varphi$ where ψ is the poloidal flux. Note that in the limit of a strong longitudinal magnetic field, the equilibrium diamagnetic flow is primarily along the poloidal direction.

In a low-$\beta = 2p/B_0^2 \sim \varepsilon^2$ plasma (B_0 is the equilibrium magnetic field strength on the axis), the equilibrium state ($\partial_t \to 0$) without MHD flows is described by the equation

$$\boldsymbol{\nabla}p = \boldsymbol{J}\times\boldsymbol{B}. \tag{5}$$

For a sufficiently small magnetic shear, the equation above is solved at leading order by [37–40]

$$R = R_0 + r\cos(\theta + r\tfrac{\delta}{a}\sin\theta) - \Delta, \quad Z = \kappa r\sin\theta \tag{6}$$

where $\kappa \sim 1$ and $\delta \sim \varepsilon$ describe plasma elongation and triangularity respectively, with the Shafranov shift $\Delta \sim \varepsilon a$ given by ($' \equiv d/dr$)

$$\Delta'' + \frac{3}{r}\Delta' + \frac{4}{1+3\kappa^2}\left(\frac{2q^2R_0p'}{rB_0^2} + \frac{2\delta}{a} - \frac{\kappa^2}{R_0}\right) = 0.$$

Here $\psi' = rB_0\kappa/q$ and $F = B_0R_0(1 - \frac{r^2(1+\kappa^2)}{2q^2R_0^2} - \frac{p'}{B_0^2})$.

If we consider the equilibrium poloidal ion velocity to be small, a MHD flow generated by $\boldsymbol{E}\times\boldsymbol{B}$ drifts may be introduced (this would rotate primarily in the poloidal direction counter to the diamagnetic flow). In this case, the equilibrium state is still described with a sufficient accuracy by Eq. (5) with $p \approx p(r)$. However, the main effect of this additional flow is to introduce a Doppler shift in the eigenfrequency without altering the stability properties. As such, for the sake of simplicity, we will not consider MHD flows at equilibrium.

Thus, introducing the rectified angle $\theta = \vartheta + \lambda(r,\vartheta)$ with $\lambda = -(r/R_0 + \Delta')\sin\vartheta$, the metric tensor elements $g_{i,j}$ in the coordinate system (r,ϑ,ϕ) with Jacobian g can be easily derived to the required accuracy by means of (6). The derivation of the stability equations will be the aim of the next section.

III. BALLOONING EQUATIONS

With an axisymmetric equilibrium, the toroidal mode n is a good quantum number, thus for any perturbed quantity $\tilde{f}$ we have

$$\tilde{f} = \sum_m f_m(r)\exp[i(m\vartheta - n\varphi) + \gamma t].$$

Under the assumption $n \gg 1$ (which also implies $m \gg 1$ with $q \sim \mathcal{O}(1)$ so that $k_{||}R_0q \ll 1$ with $k_{||}$ denoting the parallel wave vector), the perturbation is sufficiently localised so that the quantities q', p' and $s = rq'/q$ can be taken constant. It follows that adjacent resonances (each resonance denoted by r_m for a generic poloidal mode number m) are evenly spaced, i.e. $(r_{m+1} - r_m)/r_m = d =$

$1/(nqs)$. In addition, we assume that different Fourier harmonics have similar amplitude (i.e. $f_m \sim f_{m+1}$) and impose translational invariance [41]:

$$f_{m+1}(x+d) = f_m(x), \tag{7}$$

with $x = (r - r_m)/r_m$.

Hence, for a given Fourier poloidal harmonic with mode number ℓ, it is convenient to distinguish two regions: one far from its own resonance for which plasma inertia, resistivity and diamagnetism are neglected, and a second one close to r_ℓ where these effects are instead retained. Let us start analysing the far from resonance region.

A. Ideal region

Simple algebra yields [39, 42] (hereafter quantities without a tilde are assumed to take their respective equilibrium values)

$$\boldsymbol{B}\cdot\boldsymbol{\nabla}\frac{\tilde{J}^\varphi}{B^\varphi}+\tilde{\boldsymbol{B}}\cdot\boldsymbol{\nabla}\frac{J^\varphi}{B^\varphi}-\boldsymbol{J}\cdot\boldsymbol{\nabla}\frac{\tilde{B}^\varphi}{B^\varphi}-\boldsymbol{\nabla}\varphi\cdot\boldsymbol{\nabla}\frac{1}{B^\varphi}\times\boldsymbol{\nabla}\tilde{p} = I, \tag{8}$$

where the inertia operator I is given by

$$I = \boldsymbol{\nabla}\varphi\cdot\boldsymbol{\nabla}\times\frac{\rho}{B^\varphi}(\gamma\tilde{\boldsymbol{v}} + \boldsymbol{v}^*\cdot\boldsymbol{\nabla}\tilde{\boldsymbol{v}}_\perp).$$

In this region we let $I \to 0$.

Let us introduce the ballooning parameter $\alpha = -2R_0p'q^2/B_0^2$ and assume that the perturbation is localised near the plasma edge. In this region one usually has $s \sim \alpha \sim 1$, which is the standard ordering employed in the usual $s-\alpha$ model [43]. Within this model, field line bending and coupling with the nearest neighbouring sidebands arising from the first and the last two terms in (8) are of the same order. However, dealing with shaping effects, which requires higher order expansions of the metric coefficients and a more careful analysis of the poloidal couplings (i.e. for a given mode m we must retain up to the $m \pm 4$ sidebands), is significantly more difficult.

Thus, in order to simplify the algebra involved, we take $s, \alpha \ll 1$ [20, 44] and expand each term of (8) to the relevant order by including pressure and elongation driven couplings. Note that this is consistent with the equilibrium calculation presented in the previous section. The equations derived with this approximation do not differ too much from the ones obtained using the $s \sim \alpha \sim 1$ ordering. It is worth noting that the stability boundaries, at least for the ideal case, calculated in the limit $s \ll 1$ behave qualitatively in a similar manner to the ones obtained by more precise numerical computations with realistic profiles [21, 45]. This indicates that our model could be employed, to some extent, for cases with $s \sim \alpha \sim 1$ [46].

We immediately notice that because of the translational invariance (7), it is sufficient only to compute a single Fourier projection of Eq. (8), say the mth with the resonance denoted by r_m. Thus, equations (2) and (3) give $\sqrt{g}\tilde{B}^r_m = ir\kappa B_0(m/q-n)X_m$ with $\tilde{p}_m = -p'X_m$ where $X_m = \tilde{v}^r_m/\gamma$. Plasma compressibility has been neglected. Let us define

$$Y_m = (\sqrt{g}\tilde{B}^r)_m/(ir\kappa B_0).$$

We take $rd\ln\tilde{f}/dr \sim m$ so that $(m/q-n) \approx -snx$ where $nx \sim 1$ and x has been defined in Eq. (7). From the covariant toroidal projection of (1) it is easy to show that $(\tilde{B}_\varphi)_m \approx \frac{R_0p'}{B_0}X_m$, so that using $\boldsymbol{\nabla}\cdot\tilde{\boldsymbol{B}} = 0$ one has $(\sqrt{g}\tilde{B}^\vartheta)_m = i/m(\sqrt{g}\tilde{B}^r)'_m$.

The equation for the perturbation in the ideal region is obtained by multiplying (8) by $\sqrt{g}$ and selecting the mth Fourier component. Couplings between the nearest $m \pm 1$ harmonics are generated by the last term on the left hand side in (8), whereas the third one, which also combines with the fourth, is associated with the magnetic well [28, 29]. Additional elongation driven couplings with the $m \pm 2$ harmonics arise from the first term which also yields the usual Newcomb term [47]. Finally, the term proportional to the equilibrium current density gradient can be neglected. Thus, under the assumption that the mode is localised near the plasma edge for which $r \approx r_m \approx a$, we eventually obtain

$$\frac{d}{dx}\left(x^2\frac{dX_m}{dx}\right) - (m^2x^2 + \tfrac{\bar{\alpha}}{s^2}U)X_m + \tfrac{\bar{\alpha}}{2ms^2}\sum_{\ell=m\pm1}\left(mX_\ell \pm \frac{dX_\ell}{dx}\right) - \tfrac{x}{2ns}\left(\tfrac{\kappa^2-1}{\kappa^2+1}\right)\sum_{\ell=m\pm2}\left(\frac{d^2Y_\ell}{dx^2} \pm 2m\frac{dY_\ell}{dx} + m^2Y_\ell\right) = 0, \tag{9}$$

where here $Y_\ell = (\ell/q-n)X_\ell$, $\bar{\alpha} = 2\alpha/(1+\kappa^2)$ and

$$U = \frac{a}{2R_0}\left(\frac{1+7\kappa^2}{1+3\kappa^2} - \frac{1+\kappa^2}{q^2}\right) + \bar{\alpha}\frac{1+\kappa^2}{1+3\kappa^2} + \frac{3\delta(\kappa^2-1)}{1+3\kappa^2}.$$

In the limit $s^2 \sim \alpha$ [20, 44] the term U in equation (9) is formally smaller compared to other contributions, which are all of the same order. However, in experiments both aspect ratio and shaping parameters, i.e. κ and δ, may take values not too small compared to unity, suggesting that such corrections may enter the problem to leading order. As such, we retain the U term. It is also worth pointing out that the ratio of poloidal over radial derivatives in (9) is expected to scale as $md \sim 1/s$, and, although the magnetic shear is supposed to be small (cf. Sec. II), both contributions are taken into account. Hence, we en-

visage that our model could be potentially extended to $s \sim 1$ cases. A method for solving (9) with $s \sim 1$ is given in Ref. [48].

We now Fourier decompose the displacement X_m by defining $X_m^\dagger(k) = \int_{-\infty}^{\infty} dx X_m(x) \exp(-ikx)$, and take the kth moment of equation (9). Hereafter the dagger symbol will denote a k-space Fourier transformed quantity. By exploiting the radial symmetry of the perturbation given by (7) with $m \approx nq$, after some straightforward algebra we finally obtain

$$\frac{d}{dy}\Big\{[1+y^2+\left(\tfrac{\kappa^2-1}{\kappa^2+1}\right)(1+y^2-2h^2(y))]\frac{dX_m^\dagger}{dy}\Big\}+ \frac{\bar\alpha}{s^2}[h(y)-U]X_m^\dagger = 0, \tag{10}$$

having defined $h(y) = y\sin\frac{y}{s}+\cos\frac{y}{s}$ and $y = k/m$. Equation (10) features two length scales, the short one being contained in the oscillating coefficients of the function h. The solution of the equation above can be obtained by means of the *averaging method* [49–52] (a very readable account of this method is given in Refs. [35, 53]).

Let us define $e = (\kappa^2-1)/(\kappa^2+1)$ and $\chi = y/s$. By introducing the smallness parameter λ, we set [20, 53]

$$e \sim \alpha \sim \lambda, \quad s \sim \delta \sim \lambda^2, \quad \varepsilon \sim \lambda^3,$$

and expand the function $X_m^\dagger$ as follows:

$$X_m^\dagger = \xi_0(y) + \lambda\xi_1(y,\chi) + \lambda^2\xi_2(y,\chi) + \dots, \tag{11}$$

with the requirement that the functions $\xi_1, \xi_2, \dots$ vanish when averaged in the variable χ over a period of 2π. Thus, writing $d/dy \to \partial_y + \frac{1}{s}\partial_\chi$, equation (10) is solved order by order in λ, from λ^{-3} to λ, providing an expression for ξ_i $(i = 1, 2, 3)$. These are then plugged into the zeroth order (in λ) of (9), and averaging over χ yields an equation for ξ_0. With the help of computer assisted algebra tools [54], the final result reads [20, 28]

$$\frac{d}{dy}\Big[(1+y^2)\frac{d\xi_0}{dy}\Big] - \Big[\nu(\nu+1) - \frac{b^2}{1+y^2}\Big]\xi_0 = 0, \tag{12}$$

with $\nu(\nu+1) = \frac{\alpha}{s^2}[\varepsilon(1-1/q^2)+\frac{3}{2}e\delta-\frac{\alpha}{8}e^2]$ and $b^2 = \frac{\alpha^2}{s} - \frac{7}{32}\frac{\alpha^4}{s^2}$. We shall restrict our attention to the case $0 < \nu < 1/2$, i.e. for resistive interchange stable configurations. If we allowed $s \sim \alpha \sim 1$ [43] in the derivation of the mode equation (9), the averaging procedure would have come to an equation similar to (12) with the last term on the lhs replaced by $(2\alpha^2/s - \frac{3}{8}\alpha^4/s^2)/(1+y^2)^2$ [46, 53]. This fully provides a description of the perturbation dynamics in the ideal region. In the next subsection the derivation of the layer equation is presented.

B. Inertial-resistive layer

Let us set our analysis in proximity of r_m and take $d/dx \gg m$. Assuming that $\boldsymbol{\nabla}\cdot\boldsymbol{v}_i \approx 0$ [55], we may write $\tilde\rho_m = -\rho' X_m$ and $\tilde p_{im} = -p_i' X_m$ where the ion pressure equation is given by (3) with the replacements $p \to p_i$ and $\boldsymbol{v} \to \boldsymbol{v}_i$. Moreover, it easily follows that $(\tilde v_\varphi)_{m\pm1} = \frac{1}{im}R_0 q(\gamma + im\omega_i)\frac{dX_m}{dx}$ with $\omega_i = m_i p_i'/(e_i\rho a\kappa B_0)$. In the inertial layer, plasma compressibility must be retained so that $\tilde p_{m\pm1} = -p' X_{m\pm1} + \delta p_{m\pm1}$ where $\delta p_{m\pm1}$ are obtained from the parallel projection of (1) reading at leading order

$$\delta p_{m\pm1} = \pm\frac{R_0\rho q^2}{m}\frac{d}{dx}[\gamma(\gamma+im\omega_i)X_m] + p'(X_{m\pm1} \mp qY_{m\pm1}).$$

Neglecting resistivity fluctuations in (2) under the assumption that the perturbation varies sufficiently rapidly in the radial direction, we obtain with the required accuracy

$$[1 + Hy^2(1+e\cos\tfrac{2y}{s})]Y_m^\dagger = \frac{s}{iq}\frac{dX_m^\dagger}{dy}, \tag{13}$$

where $H = m^2\eta(1+\kappa^2)/[2\kappa^2a^2(\gamma - im\omega_e)]$ and $\omega_e = \rho' T_e/(e_i\rho a\kappa B_0)$ having included elongation driven couplings.

The coupling between (8) and (13) completely describes the mode dynamics in the resistive layer. We recall that Eq. (8) must be multiplied by $\sqrt{g}$ before taking the mth poloidal Fourier harmonic. Let us focus on each individual contribution arising from (8). It it easy to see that the term proportional to the gradient of the equilibrium current density is negligible also in this region. The term proportional to the perturbed current density can be easily worked out in line with the derivation of the section before, where here the magnetic fluctuation is given by (13). The pressure driving terms, i.e. the third and fourth on the lhs of (8), yield the last term in (10) augmented by the plasma compressibility contribution, which is proportional at leading order to $\frac{d}{dx}(\delta p_{m-1} - \delta p_{m+1})$. Finally, the inertial contribution can be written as $(\sqrt{g}I)_m \propto \gamma(\gamma+im\omega_i)\frac{d^2}{dx^2}[X_m + \frac{e}{2}\sum_{\ell=m\pm2}X_\ell]$. Therefore, collating these results together and transforming to the k-space yields

$$\frac{d}{dy}\Big[f(y)\frac{dX_m^\dagger}{dy}\Big] + \frac{\bar\alpha}{s^2}\{h(y) - U - [\zeta(y) + \tfrac{(2qy)^2}{1+\kappa^2}]\Lambda^2\}X_m^\dagger - \frac{\bar\alpha}{s}\left(\frac{H\zeta(y)}{1+H\zeta(y)}\right)y\cos\tfrac{y}{s}\frac{dX_m^\dagger}{dy} = 0, \tag{14}$$

where we defined $\zeta(y) = y^2[1 + e\cos\frac{2y}{s}]$ and $\Lambda^2 = \gamma(\gamma+im\omega_i)q^2/(s^2\omega_A^2)$, $\omega_A = B_0/(R_0\sqrt{\rho})$ with the function $f(y)$ given by

$$f(y) = \frac{1+y^2+e[1+y^2-2h(y)^2]}{1+H\zeta(y)}.$$

Note that for the two-regions analysis to be valid, we require that $n^2 \ll a^2|\gamma - im\omega_e|/(s^2q^2\eta)$, where this condition must hold also when $s \sim 1$, introducing an effective

upper limit in n [26]. Thus, we may restrict our analysis to moderate n modes only.

Similarly to the derivation in the ideal region, we perform a two-scales analysis [56]. Let us employ the variable χ for the argument of the periodic coefficients in the equation above (cf. section before), and take λ as a smallness parameter. We order $H \sim \lambda^2$, $\gamma \sim m\omega_{i,e} \sim \lambda$ with $y \sim 1/\lambda$ and substitute $d/dy \to \lambda\partial_y + \frac{1}{s}\partial_\chi$. Here, no λ-ordering is introduced for magnetic shear and shaping parameters. The eigenfunction $X_m^\dagger$ is expanded in λ according to (11), and then plugged into (14) yielding an expression of the form

$$\lambda^{-1}\mathfrak{D}_{-1}(\xi_0,\xi_1) + \mathfrak{D}_0(\xi_0,\xi_1,\xi_2) + \ldots = 0.$$

It is immediate to verify that the dependence upon ξ_2 in $\mathfrak{D}_0$ is annihilated by averaging in χ over a period of 2π. The leading order of the equation above provides an expression for ξ_1. Elongation introduces complicated angular dependencies in the variable χ which are resolved by casting ξ_1 as $\xi_1 = \Xi^{(0)} + e\Xi^{(1)} + \ldots$ (obviously $\Xi^{(i)}$ must be periodic in χ) and then performing a perturbative expansion in e of the expressions $\mathfrak{D}_{-1} = 0$ and $\int_0^{2\pi}\mathfrak{D}_0 d\chi = 0$. For the accuracy required in our calculations, it is sufficient to compute $\Xi^{(j)}$ with $j = 0, 1, 2$ (this is for a correct estimate of the magnetic well). After a considerable amount of algebra, taking δ and therefore magnetic well contributions sufficiently small and expanding to second order in e gives

$$\frac{d}{dy}\left(\frac{y^2}{1+H_0y^2}\frac{d\xi_0}{dy}\right) - [\nu(\nu+1) + y^2\Lambda_i^2]\xi_0 = 0, \qquad (15)$$

with $H_0 = 2\kappa H/(1+\kappa^2)$ and

$$\Lambda_i^2 = \left(\frac{1+2(1-e)q^2}{1-e^2/2}\right)\Lambda^2 \equiv \frac{\kappa^2}{\sigma}(1+2q^2)\Lambda^2,$$

where in this expression, which defines the quantity σ, we may let q be large.

Equation (15) incorporates shaping and FLR effects in the inertial layer, and together with (12) determines the ballooning dynamics. Their solution and the associated dispersion relation are discussed in the next section.

IV. STABILITY BOUNDARIES

Throughout this section we let $m = nq$ and rescale $\omega_A \to \omega_A/\sqrt{1+2q^2}$. The solutions of Eqs. (12) and (15) are well known [24, 25, 39, 52] and from their matching over the overlapping region in y we obtain the dispersion relation. Although (12) yields even and odd solutions, we restrict our attention to even parity modes only. Thus, the dispersion relation reads [24, 36, 39]

$$\frac{1}{\lambda_H} \equiv \frac{\Gamma[\frac{1}{2}(1-b+\nu)]\Gamma[\frac{1}{2}(1+b+\nu)]\Gamma^2[-\nu-\frac{1}{2}]}{\Gamma[-\frac{1}{2}(b+\nu)]\Gamma[\frac{1}{2}(b-\nu)]\Gamma^2[\nu+\frac{1}{2}]} = (H_0Q)^{-\nu-\frac{1}{2}}\frac{Q+\nu}{Q-\nu-1}\frac{\Gamma[\frac{1}{4}(Q+3-2\nu+\nu(\nu+1)/Q)]}{\Gamma[\frac{1}{4}(Q+5+2\nu+\nu(\nu+1)/Q)]} \qquad (16)$$

where $Q = \Lambda_i/\sqrt{H_0}$ and Γ is the Gamma function [57]. Although this equation is rather complicated, some limiting cases can be identified and addressed analytically.

The ideal limit is trivially obtained by taking $Q \to \infty$, providing an expression for the mode marginal stability boundary, which, for small diamagnetic ion flow, reads [39]

$$b \approx 1 + \nu + (1-\tfrac{e}{2})q|m\omega_i|/(s\pi\omega_A).$$

The destabilising role of the elongation is evident through the weakening of the diamagnetic contribution, although its interaction with triangularity improves stability via magnetic well corrections contained in the ν term [50].

Focussing on the resistive case, we restrict our attention to three limits: one with $Q \gg 1$, a second with $Q \sim 1$, and finally a third with $Q \ll 1$.

$Q \gg 1$ regime

Let us take $\lambda_H > 0$ with $\omega_i \neq 0$ and assume that the analysis is carried out in a neighbourhood of the stability region of the ideal mode when ion diamagnetic flows are present. Expanding equation (16) for large Q yields to leading order

$$\Lambda_i^2 - 4\lambda_H^{2/(1+2\nu)} \approx \left(\frac{5}{2} - \frac{\nu}{3}\right)H_0, \qquad (17)$$

where on the right hand side we assumed $\nu \ll 1$ which holds for weak shaping with a sufficiently large aspect ratio. The marginal stability boundary of the ideal mode is recovered by setting $H_0 \to 0$. We shall stress that Eq. (17), and similarly other simplified expressions of the full dispersion relation, only picks out a limited number of all the roots generated by (16).

Let us introduce the Lundquist number $S \gg 1$ defined as $S = a^2\omega_A/\eta$ and assume q large enough. Therefore, near the stability boundary of the ideal mode with diamagnetic flows, if we substitute $\gamma \to \gamma - im\omega_i/2$ with $\gamma \ll |m\omega_i|$ in Eq. (17) we find

$$\gamma \approx \gamma_*\left[1 - \frac{\nu}{15} + \frac{\gamma_I^2}{\gamma_*^2}\right],$$

where

$$\gamma_* \approx \tfrac{\sqrt{5}}{2}[m|\omega_e + \omega_i/2|/\omega_A^3]^{-1/2}[s^2m^2/(q^2S)]^{1/2},$$
$$\gamma_I^2 \approx (1+e)[\lambda_H^{1/(1+2\nu)}s\omega_A/q]^2 - (m\omega_i/4)^2 < 0,$$

with $-\gamma_I^2 \ll \gamma_*^2$. The growth rate, which is rather fast since it scales as $1/\sqrt{S}$, decreases as λ_H is reduced. Further stabilisation, although small, is gained by ν effects. With ω_i sufficiently small, the marginal boundary is given by the following expression

$$b = 1 + \nu + \frac{q|m\omega_i|}{s\pi\omega_A}\Big(1 - \frac{e}{2} - \frac{10 s^2\omega_A^3 (mS)^{-1}}{\omega_i^2|\omega_e + \omega_i/2|}\Big). \quad (18)$$

The destabilising role of the resistivity is clearly evident, although modes with a sufficiently large n are expected to be completely suppressed by the ion diamagnetic flow. We point out that if S is large enough, the stability boundary identified by (18) is not too far away from the one of the ideal mode. This seems to indicate that a modest heating may suppress these instabilities.

Finally, it is worth noticing that if γ_I^2 is sufficiently large and negative with $\lambda_H \geq 0$ not small, the two roots with frequency $-i\omega_i/2 \pm \sqrt{\gamma_I^2}$ are both stable.

$Q \sim 1$ regime

This case holds when $|\lambda_H| \ll 1$. We first expand the right hand side of (16) to first order in $\nu \ll 1$ and then take the limit $Q - 1 \ll 1$. This yields

$$\frac{1}{\lambda_H} = \frac{2}{(Q-1)\sqrt{\pi H_0}}\Big(1 + \frac{\nu}{Q-1}\Big).$$

Note that in the resistive region $H_0 y^2 \sim \Lambda_i^2 y^2 \sim 1$ [20], so that for $y \gg 1$ we obtain $qm^2/(sS) \ll 1$. A straightforward rearrangement of the equation above gives [33, 36, 58] ($\nu/(Q-1) \ll 1$)

$$Q = 1 + \nu + 2\lambda_H/\sqrt{\pi H_0}.$$

Thus, in the limit of vanishing diamagnetic corrections, we find that the growth rate is

$$\gamma = \gamma_R\Big[1 + \frac{2}{3}\nu + \frac{4\lambda_H}{3\sqrt{\pi}}\Big(\frac{\sigma}{\kappa}\Big)^{1/6}\Big(\frac{sS}{qm^2}\Big)^{1/3}\Big], \quad (19)$$

where $\gamma_R \approx \omega_A[s^2m^2/(q^2S)]^{1/3}$. For $S \to \infty$ the stability boundary identified by (19) is $\lambda_H = 0$, in agreement with the findings of the previous section. Stability is improved as λ_H becomes more negative [33], whereas the growth rate is increased by finite magnetic well corrections when $\lambda_H = 0$. It is worth noticing that the stabilising term proportional to λ_H weakens as m increases, although the condition $qm^2/(sS) \ll 1$ must be fulfilled, thence restricting the validity of this result to the neighbourhood of the marginal stability boundary of the ideal mode.

If diamagnetic flows are allowed, the growth rate of the low frequency mode is [33]

$$\gamma = \gamma_{R*}\Big[1 + 2\nu + 4\lambda_H\sqrt{\frac{\kappa S|\omega_e|}{\pi m\omega_A}}e^{i\pi/4}\Big], \quad (20)$$

where $\gamma_{R*} \approx s^2\omega_A^3/(q^2S\omega_i\omega_e)$. Similar conclusions to the ones discussed above can be drawn regarding the stability of this mode. An approximate expression for the stability boundary can be written in a form similar to (18) with the obvious replacements. Note that this root has a rather small growth rate ($\gamma_{R*} \sim S^{-1}$) and it vanishes when $S \to \infty$. As in (19), the stabilising contributions weaken as m increases.

$Q \ll 1$ regime

Here we take $|\lambda_H| \gg 1$ with $\lambda_H < 0$, i.e. far from the ideal-MHD instability threshold. Let us first neglect diamagnetic corrections. Similarly to the regime discussed in the previous paragraph, we first expand the right hand side of equation (16) to first order in $\nu \ll 1$ and then take the limit $Q \ll 1$. This yields [27]

$$\frac{1}{|\lambda_H|} = \frac{\Gamma[\frac{3}{4}]}{\Gamma[\frac{5}{4}]} \times \sqrt{\frac{Q}{H_0}}\Big(1 + \frac{\pi\nu}{4Q}\Big). \quad (21)$$

For vanishing FLR effects $Q \sim \gamma^{3/2}$, $H_0 \sim \gamma^{-1}$, and the equation above corresponds to the one analysed in Refs. [20, 24, 25] augmented by shaping effects. If $\nu \to 0$, the stability boundary for the resistive modes is given by $b = 0$, in accordance with previous analyses [20, 22, 23]. The presence of the interchange term ν, however, introduces a threshold in $1/|\lambda_H|$ as pointed out in Refs [20, 24, 25]. An estimate of such a threshold can be found by assuming ν/Q sufficiently small, so that from (21) one obtains [20]

$$\gamma = \gamma_T\left[1 - \nu\left(\frac{|\lambda_H|}{C_0}\right)^{6/5}\left(\frac{sS\sqrt{\sigma}}{m^2q}\right)^{2/5}\right].$$

where $C_0 = (5/\pi)^{5/6}\Gamma[5/4]/\Gamma[3/4] \approx 1.09$ and

$$\gamma_T = \omega_A\left(\frac{\Gamma[5/4]}{|\lambda_H|\Gamma[3/4]}\right)^{4/5} \times \left(\frac{s^2m^6\sigma}{q^2S^3\kappa^5}\right)^{1/5}.$$

Thus, the result above yields the following expression for the stability boundary

$$|\lambda_H| = C_0\nu^{-5/6}\sigma^{-1/6}\left(\frac{m^2q}{sS}\right)^{1/3} \equiv \mathscr{A}.$$

Since $\nu \ll 1$, the right hand side of this equation could take values of order unity. Because of the complicated Gamma function dependencies in λ_H, it is desirable to identify limits which are sufficiently simple to be dealt with analytically. Hence, if the right hand side of the equation above is small, we are allowed to expand $|\lambda_H|$ to first order in ν giving

$$b = 1 + \nu - \frac{4C_0}{\pi}\nu^{-5/6}\sigma^{-1/6}\left(\frac{m^2q}{sS}\right)^{1/3}. \quad (22)$$

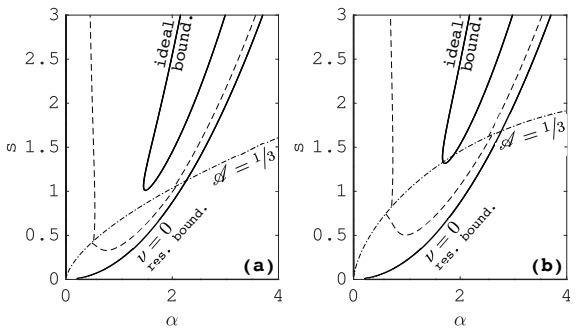

Figure 1. Ideal ($n=\infty$, non-montonic full black line) and resistive ($n=10$) stability boundaries for a circular (a) and shaped (b) tokamak with $\varepsilon=0.05$, $q=4$ and $S=10^8$. In (b) we set $\kappa=1.3$ and $\delta=0.1$. In (a) and (b), the resistive $b=0$ boundary is indicated by the monotonic thick black line. Below the $\mathscr{A}=1/3$ level (highlighted by the dot-dashed line) the resistive boundary at finite ν is computed by means of (22), whereas Eq. (23) is employed above this level both indicated by the dashed line.

It is evident that this boundary lies between the ideal marginal ($b=1+\nu$) and the resistive one with $\nu=0$ ($b=0$). Conversely, when $\mathscr{A}\sim 1$, we let $\nu\to 0$ in $|\lambda_H|$ and obtain

$$\frac{\cot(b\pi/2)}{2b}\approx\frac{1}{\pi b^2}-\frac{\pi}{12}= C_0\nu^{-5/6}\sigma^{-1/6}\left(\frac{m^2q}{sS}\right)^{1/3}, \qquad (23)$$

where the approximation above accurately holds when b is sufficiently far from unity. The ideal and the resistive $\nu=0$ stability boundaries along with the ones identified by equations (22) and (23) are shown in figure 1. It is interesting to note that plasma shaping greatly affects the opening of the RBM stability window at low pressure, whereas for ideal modes such an effect impacts more at low magnetic shear (i.e. at higher edge current densities) [59].

When strong diamagnetic effects are introduced, following the procedure outlined in Refs. [33, 34], from the dispersion relation (16) we obtain

$$\frac{\Gamma[5/4]}{\Gamma[3/4]}\approx\lambda_H^{(0)}\frac{\sqrt{Q/H_0}}{Q-1}\left(1+\nu\mathfrak{f}(Q)\right),$$

where $\lambda_H^{(0)}=\lambda_H(\nu=0)$. Note that, compared to (21) the equation above retains the $Q-1$ singularity. The function $\mathfrak{f}(Q)$ can be approximated by assuming Q small, yielding $\mathfrak{f}(Q)\approx\pi/(4Q)$. Thus, under the assumption $Q\sim\nu/Q\ll 1$ we may write

$$\frac{\Gamma[5/4]}{\Gamma[3/4]}\times\frac{1}{|\lambda_H^{(0)}|}\left(1-Q-\frac{\pi\nu}{4Q}\right)=\sqrt{\frac{Q}{H_0}}. \qquad (24)$$

It is immediate to verify that for $|\lambda_H|\gg 1$ there are three roots. Seeking the unstable root with frequency $m\omega_e$, we substitute $\gamma\to\gamma+im\omega_e$ with $\gamma\ll|m\omega_e|$. Equation (24) can be easily solved perturbatively [34], yielding for the fastest growing mode

$$\gamma\propto 1-\frac{8}{3}\Omega_*+\frac{\pi\nu}{3\Omega_*}, \qquad (25)$$

where we defined

$$\Omega_*=\left(\frac{\Gamma[5/4]}{\Gamma[3/4]|\lambda_H^{(0)}|}\right)^{2/3}\times\left[\frac{m^2q^2\kappa^2\omega_e(\omega_e+\omega_i)}{s^2\omega_A^2\sigma}\right]^{1/3}.$$

The result above suggests the destabilising effect of finite magnetic well corrections [60, 61]. However, complete stabilisation can be achieved for any m [33, 34] owing to the second term on the right hand side of (25) for λ_H sufficiently small. We also point out, that the growth rate scales as S^{-1} [33, 34] indicating that this root grows slowly and eventually disappears in the ideal limit.

Thus, having discussed the physically relevant limits of the dispersion relation (16), the aim of the next section is to link the analytical findings to experimental observations.

V. CRITICAL PRESSURE HEIGHT

As mentioned in the introduction, resistive ballooning modes are likely to be associated with type-III ELM dynamics. Hence, our aim in this section is to derive an expression for the critical pedestal pressure height beyond which RBMs appear, and link it to type-III ELM phenomenology. Type-III ELMs are usually found above the $L\to H$ boundary [7, 8] at moderate pedestal height and high collisionality [3, 9, 11, 12]. Since type-III ELMs localise at low values of edge current in the peeling-ballooning stability diagram at not too high pressure, we focus on equation (23), i.e. for a low-α and moderate s case. Noting also that the boundaries computed with $s\sim 1$ behave qualitatively as the ones obtained in the $s\ll 1$ limit [21], it might be reasonable, to some extent, to push the theory towards the $s\sim 1$ limit. Finally, because the toroidal wave number associated with type-III ELM precursors is generally not too large ($n\sim 10$) [11–14], we may drop diamagnetic corrections.

The pressure gradient appearing in the ballooning parameter α can be well approximated by

$$-\frac{dp}{dr}\approx\frac{p}{a\Delta_{ped}},$$

where $\Delta_{ped}=(a-r_{ped})/a$ is the pedestal width with r_{ped} indicating the pedestal shoulder. The quantity Δ_{ped} is estimated by means of the EPED model [31, 32, 45], in which the pedestal width scales with the pressure according to $\Delta_{ped}=Cq\beta^{1/2}/\varepsilon$ with $C\sim 0.05$ where β has to be evaluated at the pedestal top. For $T_e=T_i=T$ we have $\beta=2\mu_0 p/B^2=4\mu_0 n_e T/B^2$ where n_e is the plasma density, having restored the vacuum permeability. Note that

we accounted for the fact the EPED-pedestal width is written as a function of the poloidal flux [31, 32], whereas our expression depends upon the variable $r \sim \sqrt{\psi}$. Finally, we take the local value of the Lundquist number as an independent parameter, i.e. the value of resistivity in S is independent of the pedestal top temperature. This is consistent with the derivation in Sec. III, in which we considered the instability to be highly localised, i.e. $m \gg 1$.

As noted in the previous section, ν corrections to the ideal marginal boundary are rather weak in the region of sufficiently high magnetic shear. This, indeed, might explain why the transition temperature between type-I and type-III ELMy behaviour depends weakly upon triangularity [7]. Therefore, by writing $\alpha = q\sqrt{\beta}/C$, the boundary of the first stability region for the ideal mode with $\nu = 0$ is identified by $b = 1$ which yields $\beta \approx 1.48 \times sC^2/q^2$. Focussing on the resistive perturbation, if the ratio α^2/s is sufficiently low (low-α/high-s region), we are allowed to take $b^2 \approx \alpha^2/s$. Thus, approximating $\nu^{-5/6} \approx \alpha^{-1}(\nu/\alpha)^{-5/6}$ on the right hand side of (23), we can obtain an explicit expression for the critical pedestal pressure which reads

$$q\sqrt{\beta}/C \approx -\tau + \sqrt{12s/\pi^2 + \tau^2}, \tag{26}$$

where

$$\tau = \frac{6}{\pi} q s^{4/3} C_0 (\varepsilon + \tfrac{3}{2}e\delta)^{-5/6} \sigma^{-1/6} \left(S/n^2\right)^{-1/3},$$

having neglected the $e^2\alpha/8$ term in ν (this is because α is assumed to be small enough) with $q \gg 1$. An example of the behaviour of the stability boundary identified by (26) in the $n_e - T$ parameter space, which exhibits qualitative similarities with experimental findings [7, 8, 30], is shown in figure 2. The beneficial role of plasma shaping, i.e. vertical elongation with positive triangularity, is apparent through the upwards shift of the RBM stability boundary. We point out that type-I ELMs are likely to appear as the boundary of the ideal mode is met, thus limiting the maximum achievable pressure height [19]. As such, we argue that the boundary of the second stability region is never crossed. We stress however that diamagnetic flows may favour the accessibility to higher pressure regions. On the other hand, the RBM (and thus the type-III ELMs) threshold is a *softer* limit which can be crossed allowing higher pressure regions to be explored, until the type-I ELM boundary is reached.

We shall now briefly discuss the boundaries identified by Eqs. (18) and (22), both of which share the same structure. By taking S large, we note that although (20) yields a similar expression for the stability boundary, the growth rate associated with this mode is so small ($\sim S^{-1}$) as to be not particularly relevant in the limit of large Lundquist numbers. Hence, taking $\frac{7}{32}\alpha^2/s \ll 1$ and neglecting the $e^2\alpha/8$ term in ν, we obtain the critical pressure ($q \gg 1$)

$$q\sqrt{\beta}/C = \tfrac{71}{64}\sqrt{s} + \tfrac{1}{s}(\varepsilon + \tfrac{3}{2}e\delta) - \mathscr{U}, \tag{27}$$

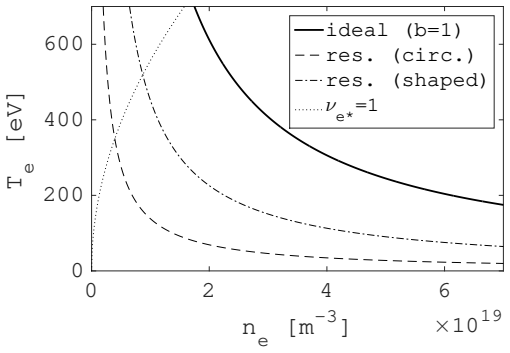

Figure 2. Boundaries for $n = \infty$ ideal ballooning (with $\nu = 0$ where only the first stability boundary is shown) and for a $n = 10$ resistive mode with $s = 1.5$, $R = 3m$, $B = 4T$, $\varepsilon = 0.1$, $q = 3$ and $S = 10^7$ for a circular and shaped ($\kappa = 1.5$ and $\delta = 0.3$) tokamak with $T_i = T_e$. The stability regions lie below each respective curve. The $\nu_{e*} = 1$ level (ν_{e*} is the electron collisionality whose definition follows Ref. [62] having used $Z_{eff} = 1$) below which (26) is expected to hold is also shown.

where from (18)

$$\mathscr{U} = -\frac{q|m\omega_i|}{\sqrt{s}\pi\omega_A}\left(1 - \frac{e}{2} - \frac{10s^2\omega_A^3(mS)^{-1}}{\omega_i^2|\omega_e + \omega_i/2|}\right),$$

while from (22) the quantity $\mathscr{U}$ can be written in a form similar to τ defined below Eq. (26) apart from some slightly different numerical coefficients. In the latter, (27) closely resembles Eq. (26) expanded to first order in τ in which the ν contribution to b has been neglected. We may drop the second term on the right hand side of (27) if the magnetic shear is sufficiently large, indicating that for the case with strong diamagnetic effects identified by Eq. (18) plasma shaping effects are of higher order.

VI. CONCLUSIONS

In this work the impact of magnetic well contributions, primarily through plasma shaping, also including finite Larmor radius effects, on the stability properties of resistive ballooning modes has been analysed. The analysis focussed on a particular choice of the perturbed displacement for which neighbouring Fourier harmonics are translationally invariant (cf. (7)). By performing a two scale analysis, with a careful ordering of magnetic shear and shaping contributions, it has been possible to derive an averaged ballooning equation in the ideal and inertial-resistive regions. By matching the two solutions we obtained a dispersion relation which has been analysed for various limiting cases.

When finite Larmor radius corrections are negligible, stability is generally improved for a vertically elongated cross section with positive triangularity, whereas close to the ideal marginal boundary the growth rate tends to be

increased. Diamagnetic effects have a strong stabilising influence altering significantly the growth scaling with the Lundquist number. Various roots and their corresponding stability boundaries, have been identified.

Finally, in the limit of negligible diamagnetic effects, which appears to be appropriate for plasmas near the $L \to H$ transition, we derived by means of the EPED model an expression of the RBM critical pressure value at the pedestal top. This seems to compare favourably with the type-III ELM dynamics, and thus could provide a sensible physical interpretation for such phenomenon.

We point out that our study is limited to the $n \gg 1$ case, for which (7) holds. Therefore, different results might be expected if slightly alternative forms of the fluid perturbation are considered [63]. Note also that in our calculations we assumed that n is not too large in order for the two scales analysis to hold. As such, several effects, which may become important for finite n perturbations, have been neglected (e.g. resistivity variations across the pedestal region). Furthermore, we envisage that for n finite a variational approach, which might be more easily tackled via numerical methods, would be more appropriate.

ACKNOWLEDGEMENTS

This work has been carried out within the framework of the EUROfusion Consortium and has received funding from Enabling Research grant on Reactor Relevant Pedestals (ENR-MFE19.CCFE-04-T002-D001), the Euratom research and training programme 2014–2018 and 2019–2020 under Grant agreement No. 633053 and from the RCUK [Grant No. EP/T012250/1]. To obtain further information on the data and models underlying this paper please contact PublicationsManager@ukaea.uk. The views and opinions expressed herein do not necessarily reflect those of the European Commission. This work was supported in part by the Swiss National Science Foundation.

[1] Wagner F *et al.* 1984 *Phys. Rev. Lett.* **53** 1453
[2] Keilhacker M 1987 *Plasma Phys. Control. Fusion* **29** 1401
[3] Leonard A W 2014 *Phys. Plasmas* **21** 090501
[4] Rapp J *et al.* 2005 *J. Nucl. Mater.* **337-339** 826
[5] Rapp J *et al.* 2009 *Nucl. Fusion* **49** 095012
[6] Rapp J *et al.* 2012 *Nucl. Fusion* **52** 122002
[7] Sartori R *et al.* 2004 *Plasma Phys. Control. Fusion* **46** 723
[8] ITER Physics Expert Group on Confinement and Transport *et al* 1999 *Nucl. Fusion* **39** 2175
[9] Doyle E J *et al.* 1991 *Phys. Fluids B* **3** 2300
[10] Oyama N *et al.* 2006 *Plasma Phys. Control. Fusion* **48** A171
[11] Connor J W 1998 *Plasma Phys. Control. Fusion* **40** 531
[12] Zohm H 1996 *Plasma Phys. Control. Fusion* **38** 105
[13] Kass T *et al.* 1998 *Nucl. Fusion* **38** 111
[14] Poli F M *et al.* 2008 *Plasma Phys. Control. Fusion* **50** 095009
[15] Xu X Q *et al.* 2011 *Nucl. Fusion* **51** 103040
[16] Orain F *et al.* 2015 *Phys. Rev. Lett.* **114** 035001
[17] Kleiner A *et al.* 2021 *Nucl. Fusion* **61** 064002
[18] Pogutse O P *et al.* 1999 *26th EPS Conf. on Plasma Physics (European Physical Society, Maastricht, Netherlands, 14-18 June 1999)* **23J** 249
[19] Chankin A V and Saibene G 1999 *Plasma Phys. Control. Fusion* **41** 913
[20] Strauss H R 1981 *Phys. Fluids* **24** 2004
[21] Connor J W *et al.* 1998 *Phys. Plasmas* **5** 2687
[22] Sykes A *et al.* 1987 *Plasma Phys. Control. Fusion* **29** 719
[23] Bishop C M *et al.* 1990 *Phys. Fluids B* **2** 3052
[24] Correa-Restrepo D 1982 *Z. Naturf. a* **37** 848
[25] Correa-Restrepo D 1985 *Plasma Phys. Control. Fusion* **27** 565
[26] Drake J F and Antonsen T M 1985 *Phys. Fluids* **28** 544
[27] Glasser A H *et al.* 1975 *Phys. Fluids* **18** 875
[28] Krymskii A M 1981 *Sov. J. Plasma Phys.* **7** 371
[29] Lütjens H *et al.* 1992 *Nucl. Fusion* **32** 1625
[30] Saibene G *et al.* 2002 *Plasma Phys. Control. Fusion* **44** 1769
[31] Snyder P B *et al.* 2009 *Phys. Plasmas* **16** 056118
[32] Snyder P B *et al.* 2011 *Nucl. Fusion* **51** 103016
[33] Migliuolo S 1993 *Nucl. Fusion* **33** 1721
[34] Migliuolo S *et al.* 1991 *Phys. Fluids B* **3** 1338
[35] Hazeltine R D and Meiss J D 1992 *Plasma Confinement* (Redwood City: Addison-Wesley Publishing Company)
[36] Ara G *et al.* 1978 *Ann. Phys.* **112** 443
[37] Miller R L *et al.* 1998 *Phys. Plasmas* **5** 973
[38] Shafranov V D and Yurchenko E I 1968 *Nucl. Fusion* **8** 329
[39] Mikhailovskii A B 1998 *Instabilities in a Confined Plasma* (Bristol: IOP)
[40] Brunetti D *et al.* 2020 *Plasma Phys. Control. Fusion* **62** 115005
[41] Tsang K T 1981 *Phys. Fluids* **24** 2017
[42] Coppi B *et al.* 1966 *Nucl. Fusion* **6** 101
[43] Connor J W *et al.* 1978 *Phys. Rev. Lett.* **40** 396
[44] Mikhailovskii A B and Yurchenko E I 1982 *Plasma Physics* **24** 977
[45] Snyder P B *et al.* 2002 *Phys. Plasmas* **9** 2037
[46] Fu G Y *et al.* 1990 *Phys. Fluids B* **2** 2623
[47] Newcomb W 1960 *Ann. Phys.* **10** 232
[48] Connor J W *et al.* 1991 *Phys. Plasmas* **3** 1539
[49] Lortz D and Nührenberg J 1979 *Nucl. Fusion* **19** 1207
[50] Pogutse O P *et al.* 1980 *Sov. J. Plasma Phys.* **6** 341
[51] Coppi B *et al.* 1980 *Phys. Rev. Lett.* **44** 990
[52] Antonsen Jr T M *et al.* 1982 *Plasma Physics* **24** 197
[53] Connor J W *et al.* 2016 *Plasma Phys. Control. Fusion* **58** 085002
[54] Wolfram Research Inc. 2010 Mathematica Version 6.0 (Champaign, IL: Wolfram Research Inc)
[55] Hazeltine R D and Ross D 1978 *Phys. Fluids* **21** 1140
[56] Hastie R J *et al.* 2003 *Phys. Plasmas* **10** 4405

[57] Abramowitz M and Stegun I A 1964 *Handbook of Mathematical Functions* (New York: Dover)
[58] Porcelli F 1987 *Phys. Fluids* **30** 1734
[59] Snyder P B *et al.* 2004 *Nucl. Fusion* **44** 320
[60] Riva F *et al.* 2017 *Plasma Phys. Control. Fusion* **59** 035001
[61] Seto H *et al.* 2018 *Plasma Fusion Res.* **13** 3403086
[62] Sauter O *et al.* 1999 *Phys. Plasmas* **6** 2834
[63] Tsang K T and Catto P J 1977 *Phys. Rev. Lett.* **39** 1664